Remote Sensing of Environment 258 (2021) 112385

Contents lists available at ScienceDirect

Remote Sensing of Environment

journal homepage: www.elsevier.com/locate/rse

Identifying the effects of chronic saltwater intrusion in coastal floodplain swamps using remote sensing

Elliott White Jr [a,*], David Kaplan [b]

[a] Environmental Sciences Department, University of Virginia, Charlottesville, VA 22903, USA
[b] Engineering School of Sustainable Infrastructure and Environment, Environmental Engineering Sciences Department, University of Florida, Gainesville, FL 32611, USA

ARTICLE INFO

Keywords:
Saltwater intrusion
Sea level rise
Coastal floodplain swamps
Remote sensing
EVI
MODIS
Climate change
Google Earth Engine
Ghost Forest

ABSTRACT

Coastal floodplain swamps (CFS) are an important part of the coastal wetland mosaic, however they are threatened due to accelerated rates of sea level rise and saltwater intrusion (SWI). While remote sensing-based detection of wholesale coastal ecosystem shifts (i.e., from forest to marsh) are relatively straightforward, assessments of chronic, low-level SWI into CFS using remote sensing have yet to be developed and can provide a critical early-warning signal of ecosystem deterioration. In this study, we developed nine ecologically-based hypotheses to test whether remote sensing data could be used to reliably detect the presence of CFS experiencing SWI. Hypotheses were motivated by field- and literature-based understanding of the phenological and vegetative dynamics of CFS experiencing SWI relative to unimpacted, control systems. Hypotheses were organized into two primary groups: those that analyzed differences in summary measures (e.g., median and distribution) between SWI-impacted and unimpacted control sites and those that examined timeseries trends (e.g., sign and magnitude of slope). The enhanced vegetation index (EVI) was used as a proxy for production/biomass and was generated using MODIS surface reflectance data spanning 2000 to 2018. Experimental sites ($n = 8$) were selected from an existing network of long-term monitoring sites and included 4 pairs of impacted/non-impacted CFS across the northern Gulf of Mexico from Texas to Florida. The four best-supported hypotheses (81% across all sties) all used summary statistics, indicating that there were significant differences in the EVI of CFS experiencing chronic, low-level SWI compared to controls. These hypotheses were tested using data across a large and diverse region, supporting their implementation by researchers and managers seeking to identify CFS undergoing the first phases of SWI. In contrast, hypotheses that assessed CFS change over time were poorly supported, likely due to the slow and variable pace of ecological change, relatively short remote sensing data record, and/or specific site histories. Overall, these results show that remote sensing data can be used to identify differences in CFS vegetation associated with long-term, low-level SWI, but further methodological advancements are needed to reliably detect the temporal transition process.

1. Introduction

The coastal wetland mosaic is a complex of wetland types (swamps, marshes, and mangroves) that inhabit the coastal margin and are patterned along abiotic gradients (e.g., hydroperiod, salinity, and nutrient concentration). Directional changes to abiotic gradients and disturbance frequency can alter coastal wetland structure and function and drive wholesale ecosystem transitions (Hong et al., 2019; Kirwan and Gedan, 2019; Klein et al., 2005; Odland and del Moral, 2002; Reaver et al., 2019). Flood frequency and salinity gradients are two important drivers of coastal wetland distribution (Craft et al., 2009; Kirwan et al., 2016; McKee and Mendelssohn, 1989; Middleton and Souter, 2017) that are closely linked to global climate change and sea-level rise (SLR), making them important drivers of coastal wetland change. These stressors have been widely demonstrated to cause shifts in the community structure and composition of both saline (Angelini and Silliman, 2012; Brinson et al., 1995; Brinson et al., 1985; Langston et al., 2017; Liu et al., 2017) and freshwater (Chen et al., 2016; Knighton et al., 1991; Neubauer, 2011; Rasmussen et al., 2013; Rice et al., 2012; White and Kaplan, 2017) coastal wetlands.

Among coastal wetland types, coastal floodplain swamps (CFS) are freshwater wetlands characterized by woody, flood-tolerant tree species

* Corresponding author.
E-mail address: eew5x@virginia.edu (E. White).

https://doi.org/10.1016/j.rse.2021.112385
Received 31 July 2020; Received in revised form 26 December 2020; Accepted 2 March 2021
Available online 12 March 2021

(Cowardin et al., 1979; Mitsch and Gosselink, 2015). CFS provide US $1.5 T yr^{-1} in ecosystem services globally (Costanza et al., 2014), including nutrient removal, storm surge attenuation, and carbon sequestration (Blair et al., 2015; Engle, 2011). The ecological integrity of CFS and their ability to provide these services is threatened by accelerating SLR and saltwater intrusion (SWI). While many saline coastal wetlands (i.e., marshes and mangroves) have demonstrated the ability to "keep up" with SLR via accretion and soil elevation change (Cahoon et al., 2019; Kirwan et al., 2016; Morris et al., 2002), rates of elevation change in CFS (1.3–2.2 mm yr^{-1}; Craft, 2012; Doyle et al., 2007) are below the current global mean SLR rate of 3.2 mm yr^{-1} (Church and White, 2011; Horton et al., 2014). Saltwater intrusion can also lead directly to absolute losses in elevation (Charles et al., 2019; Krauss et al., 2020; Krauss et al., 2016). Finally, fluctuations in riverine hydrology play a major structuring role in CFS (Robertson and Augspurger, 1999; Yin, 1998; Zeiringer et al., 2018) making them vulnerable to SWI driven by natural and anthropogenic drivers in the watershed (White and Kaplan, 2017). Taken together, changes in riverine and coastal hydrology have led to the deterioration or conversion of CFS on a global scale (Kirwan and Gedan, 2019).

One of the most visible indicators of SWI impacts on CFS is the presence of "ghost forests" along coastal margins (Kaplan et al., 2010; Kirwan and Gedan, 2019; Langston et al., 2017; Schieder et al., 2018). The presence of ghost forests is visually apparent in the field (standing dead trees and abundant herbaceous groundcover) where chronic SWI is present. However, while the effects of acute SWI at specific sites can be observed through resource-intensive field campaigns (Conner, 1995; Magnuson, 1990; Steyer et al., 2007), identifying chronic SWI stress associated with SLR and/or long-term flow alteration requires adequate time, funding, equipment, and long-term interest to sustain monitoring and data collection efforts (Franklin, 1989; Lovett et al., 2007; Strayer et al., 1986). Until recently there have been few studies quantifying the range and extent of CFS loss (but see Raabe and Stumpf, 2016; Ross et al., 1994; Schieder et al., 2018; Ury et al., 2020), and no studies of which we are aware that attempt to identify early-warning signals of CFS deterioration preceding wholesale conversion to marsh. In this challenging context, remote sensing (RS) offers the opportunity to better understand the long-term effects of chronic SWI on CFS over large spatiotemporal scales by capitalizing on the wealth of global, satellite-based, multispectral imagery datasets that have been compiled in the past several decades (Alonso et al., 2016; Ji et al., 2001; Li and Weng, 2007; Moran et al., 1997). Unlike previous land cover/land use change studies on coastal forested systems, which primarily rely on forest-type classification (Goldberg et al., 2020; Magolan and Halls, 2020; Taillie et al., 2020), here we focus on the unique physiological and phenological characteristics of CFS vegetation that arise due to chronic SWI.

An understanding of the physiological and phenological characteristics of CFS vegetation is useful for identifying potential RS approaches to detecting the effects of chronic, low-level SWI. Coastal floodplain swamps are most often populated by freshwater, needle- and broad-leafed, deciduous canopy trees (i.e. *Taxodium distichum*, *Nyssa spp.*, *Fraxinus spp.*), which characteristically have a leaf-out period in early spring, during which there is active growth, and a leafless period in winter, during which they are dormant (Brinson et al., 1980; Krauss et al., 2015). Additionally, under characteristic freshwater conditions, CFS have relatively sparse understory vegetation (Huenneke and Sharitz, 1986; Krauss et al., 2009), while CFS undergoing SWI are often colonized by an herbaceous understory of salt-tolerant species, which persist through the dormant season (Fig. 1). Notably, the dynamics of non-wetland deciduous forests have been routinely and accurately observed using remote sensing (Duchemin et al., 1999; Nakaji et al., 2011; Wang et al., 2005). Using remote sensing data we thus expect that CFS impacted by SWI will show muted seasonal variation in greenness due to reduced canopy productivity during the growing season and increased greenness during the dormant season due to additional understory vegetation.

Given our conceptual understanding and expectations about the phenology and growth dynamics of SWI-impacted vs. unimpacted CFS, we developed a set of nine hypotheses (Table 1 and described in detail in Section 2.2) to test the ability of remote sensing to identify SWI impacts in CFS. Our overall goal was to determine which of these nine hypotheses, if any, would be useful for identifying chronic SWI impacts on CFS using only remote sensing data. To do so, we tested each hypothesis across a network of previously established CFS sites along the northern Gulf of Mexico. Available data included records of vegetation and shallow groundwater salinity, allowing us to assign sites a priori as SWI-

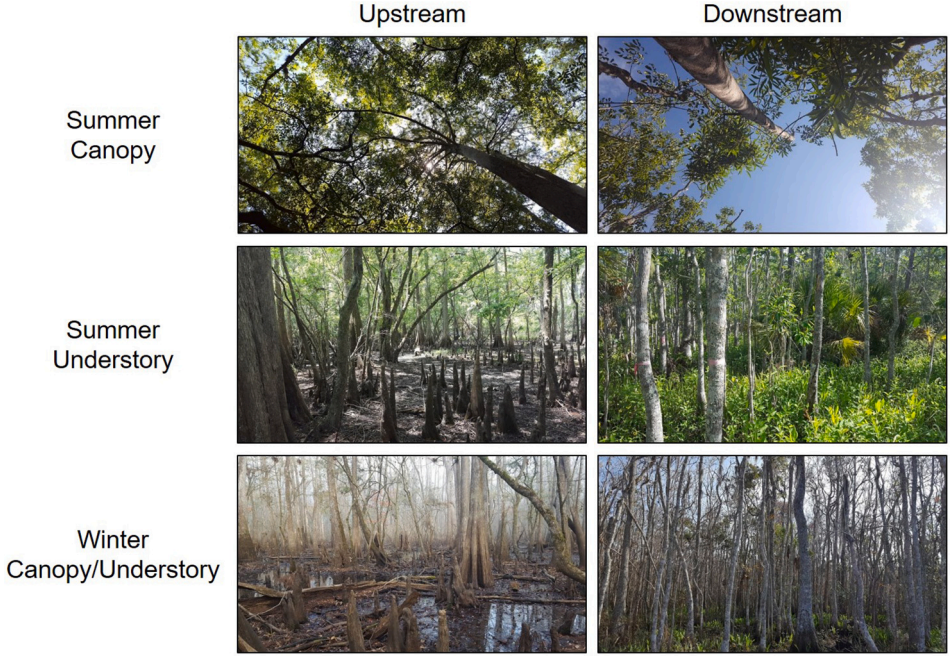

Fig. 1. Photographs of coastal floodplain swamps along the Suwannee River (FL) illustrating differences in seasonal phenology and growth dynamics between upstream (control) and downstream (saltwater intrusion-impacted) sites.

Table 1
Hypotheses developed to identify the effects of saltwater intrusion (SWI) on coastal floodplain swamps (CFS) using remote sensing. In the table below, EVI is the Enhanced Vegetation Index; UP/DOWN refer to non-impacted *upstream* sites and SWI-impacted *downstream* sites; TREND refers to de-seasonalized change over time, and GS/DS refer to *growing* and *dormant* seasons.

Hypothesis	Ecological Rationale	Test
H_{1A}: $\tilde{X}EVI_{DOWN} < \tilde{X}EVI_{UP}$	Lower EVI at downstream sites indicates the presence of a stressor	MWU
H_{1B}: $X \sim EVI_{DOWN} \neq X \sim EVI_{UP}$	Differences in distribution imply changes to phenological patterns	KS
H_{2A}: Slope $EVI_{DOWN} < 0$	Long-term negative slope at downstream sites imply SWI-induced stress	MK, SS
H_{2C}: Slope $EVI_{Trend, DOWN} < 0$	A declining de-seasonalized trend indicates a long-term change in EVI	MK, SS
H_{2B}: Slope $EVI_{DOWN:UP} < 0$	The ratio between upstream and downstream sites accounts for any shared regional stressors; a declining slope indicates a local stressor is affecting the downstream site	MK, SS
H_{3A}: $\tilde{X}EVI_{GS,DOWN} < \tilde{X}EVI_{GS,UP}$	Lower growing-season EVI can indicate the effect of SWI stress on peak biomass/ productivity	MWU
H_{3B}: $\tilde{X}EVI_{DS,DOWN} > \tilde{X}EVI_{DS,UP}$	Higher dormant-season EVI may indicate the presence of salt-tolerant herbaceous understory species (succession)	MWU
H_{3C}: $\tilde{X}EVI_{GS:DS,DOWN} < \tilde{X}EVI_{GS:DS,UP}$	Lower GS:DS ratios imply a decrease in seasonal variation (phenological change)	MWU
H_{3D}: Slope $EVI_{GS:DS, DOWN} < 0$	A negative slope indicates a significant impact on growing season EVI values compared to those of the dormant period	MK, SS

The symbols $\tilde{X}$ and $X \sim$ represent median and distribution, respectively. Statistical techniques and test used in this study are abbreviated as follows: Mann-Whitney U (MWU), Kolmogorov-Smirnov (KS), Mann-Kendall (MK), and Sen's Slope (SS).

impacted (or not) for the purpose of hypothesis testing in this work.

2. Methods

2.1. Study sites, vegetation, and hydrology

The sites used in this study were distributed across the northern Gulf of Mexico in Texas ($n = 2$), Louisiana ($n = 2$), and Florida ($n = 4$; Fig. S1). Sites were generally paired along the same river reach (i.e., one downstream, SWI-impacted site; one upstream, un-impacted site), except for the Louisiana region, which were located in different hydrologic basins due to data limitations. Downstream sites were identified as SWI-impacted based on groundwater salinity measurements from sensors deployed in each location (Table 2; described further in the Supplemental Material), however all downstream sites were dominated by woody canopy (not herbaceous marsh) species. Distances between upstream and downstream sites were selected to reduce the effects of differential regional drivers of stress (i.e., rainfall, freshwater flow, or extreme temperatures) and differences in primary production associated with changes in latitude (Middleton and McKee 2004), while still maintaining a distinct freshwater to brackish salinity gradient. Of the eight sites, six came from a network of sites established by the authors and collaborators for the purposes of monitoring the long-term effects of chronic SWI on CFS vegetation. The remaining two sites consisted of: 1) an upstream site in Louisiana site selected based on its proximity to a Louisiana Coastwide Reference Monitoring System (CRMS) station, which records vegetation, hydrology, and water quality data; and 2) an upstream site in Texas selected based on its proximity to a United States Geological Survey (USGS) river gage and the description of the floodplain vegetation by Hall and Harcombe (1998). All sites are located on state or federally protected lands, minimizing the effects of direct anthropogenic impacts.

In general, both upstream and downstream sites were dominated by woody canopy vegetation that are characteristic of CFS (i.e., *Taxodium distichum*, *Nyssa spp.*, *Fraxinus spp.*), however downstream sites had a greater density of salt-tolerant understory vegetation. There is little to no seasonal variation in understory vegetation. Distance from the coast was estimated for each site by taking the shortest route through water to the coastline. Detailed site descriptions, including site histories, vegetation, and a summary of relevant hydrology and water quality are provided in the Supplemental Material. Hydrologic and water quality data were retrieved from multiple sources. On-site groundwater data were acquired from a network of groundwater wells established at 24 sites across the Northern Gulf of Mexico (including six of the sites used in this study). Shallow groundwater wells were slotted below the soil surface, installed to an average depth of one meter, backfilled with sand, and sealed with bentonite clay at the surface. Wells were outfitted with a conductivity-temperature-depth probe (Aqua Troll 200, In-Situ, Fort Collins, CO or CTD Diver, Van Essen Instruments, Mukilteo, WA), which recorded data at 15-min intervals. Sensors were downloaded during quarterly visits and continuously recorded data for three to four years, depending on location. Pressure data from each sensor were corrected for atmospheric pressure to derive water level, and conductivity data were converted to salinity following Schemel (2001). The SE Louisiana upstream site water level and salinity data are from CRMS and span from 2008 to 2018. The Neches upstream site does not have any site level hydrology or salinity data.

Table 2
Summary of distance from coast, elevation, water level and salinity for each site in the study. Upstream/downstream sites were paired across four regions.

Regions	Distance Upstream (km)	Mean (± SD) Elevation (m)	Mean (±SD) Water Level (cm)	Mean (±SD) Salinity (ppt)
Suwannee				
Upstream	42	22.19 ± 4.01	−2.66 ± 30.34	0.34 ± 0.18
Downstream	5	13.83 ± 2.19	−3.33 ± 10.81	0.78 ± 0.41
Big Bend				
Upstream	10	15.23 ± 1.27	−3.57 ± 15.64	0.13 ± 0.07
Downstream	6	12.48 ± 1.61	−12.4 ± 27.62	1.79 ± 0.75
SE Louisiana				
Upstream	72	6.36 ± 1.72	6.1 ± 17.91	0.15 ± 0.05
Downstream	77	13.71 ± 2.01	3.94 ± 10.83	1.11 ± 0.23
Neches				
Upstream	124	25.03 ± 1.83	NA	NA
Downstream	74	8.4 ± 1.8	30.61 ± 52.87	4.09 ± 0.73

River discharge and salinity (where available) data for each region were retrieved from the USGS National Water Information System (NWIS) via the waterData package developed for R (Ryberg and Vecchia, 2012). Gages were selected based upon proximity to sites, and their locations; gage names and unique NWIS IDs are summarized in Fig. S2 and Table S1. Data are presented as retrieved from the waterData package, with one exception: Suwannee River salinity at Gopher River is available for both top and bottom of the water column; we present the average of those values. Neches River salinity data at the Saltwater Barrier were provided by the Lower Neches Valley Authority (LNVA) as specific conductance in microSiemens/cm, which were converted to salinity based on Schemel (2001).

2.2. Hypothesis formation

Hypotheses were motivated by expected differences in statistical measures and temporal patterns of greenness (as measured by the enhanced vegetation index; EVI) between downstream, SWI-impacted sites (transitioning to marsh), and upstream, unimpacted sites (fully forested). Hypotheses were based on existing literature and organized

around three general statistical characteristics: 1) overall EVI median and distribution ($H_{1A\text{-}B}$); 2) long-term EVI trends ($H_{2A\text{-}C}$); and 3) differential impacts of SWI on growing season versus dormant season EVI ($H_{3A—D}$). Specifically, we expected long-term median greenness to be lower at downstream, SWI-impacted sites (H_{1A}) due to declines in biomass and general health of CFS canopy species (Fig. 2A; Cormier et al., 2012; Krauss et al., 2009; Pierfelice et al., 2015). We also expected differences in EVI distributions between upstream and downstream sites (H_{1B}) due to reduced peak growing season EVI and elevated dormant-season EVI driven by the transgression of perennial, salt-tolerant herbaceous species into the understory (Fig. 2A-B; Huenneke and Sharitz, 1986; Krauss et al., 2009). Regarding temporal trends, we expected EVI to decline over time at downstream sites, whether assessed using seasonally varying or de-seasonalized data ($H_{2A,B}$; Fig. 2C). Since these tests do not account for regional stressors that could cause EVI to decline in both upstream and downstream sites independent of SWI, we also tested for temporal trends in the ratio of EVI in downstream vs. upstream sites ($EVI_{DOWN:UP}$), hypothesizing that there would be a decline in this ratio (H_{2C}) if SWI was specifically affecting the downstream vegetative community.

Regarding seasonal dynamics, CFS exhibit distinct seasonality that can be generally partitioned into four phases: 1) the "dormant season" where all deciduous trees have lost their leaves due to senescence, resulting in yearly minimum EVI values (December through February); 2) the "green-up/leaf out" period, which is evidenced by a rapid increase in EVI (March); 3) "peak growing season" with maximum EVI values (April to June); and 4) "stable decline" where EVI values steadily decline as trees begin enter maintenance mode and/or senesce (July to November). These seasonal phases are based on recent research of deciduous forest annual phenology (Xie and Wilson, 2020) and a preliminary review of our data. As with H_1, we expected that the average growing season EVI (EVI_{GS}) would be lower at downstream sites relative to upstream sites (H_{3A}) due to SWI effects on peak primary production and overall canopy health (Allen et al., 1997; Conner et al., 1997).

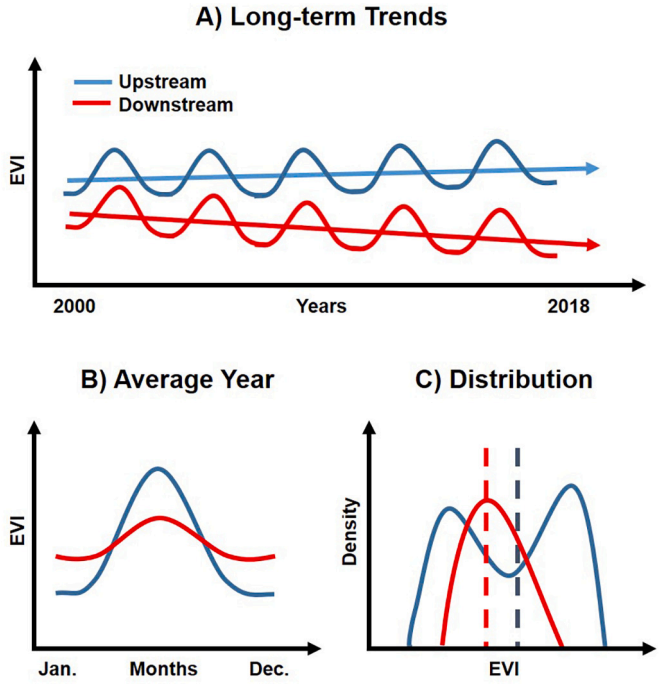

Fig. 2. Conceptual expectations for Enhanced Vegetation Index (EVI) upon which hypotheses were based, including: (A) a decline in long-term EVI at downstream, salt-impacted sites; (B) lower growing season EVI and higher dormant season EVI downstream; and (C) lower median EVI and a shift toward a unimodal distribution at downstream sites.

Conversely, the average dormant season EVI (EVI_{DS}) should be higher at downstream sites compared to upstream sites (H_{3B}) due to the presence of perennial, salt-tolerant herbaceous species in the understory. Following from these expectations, we also hypothesized that the ratio of average growing to dormant season EVI ($EVI_{GS:DS}$) would be lower at downstream sites (H_{3C}) and that this ratio would decline over time in downstream systems experiencing the persistent effects of chronic SWI (H_{3D}).

2.3. Remote sensing data

The cloud computing platform Google Earth Engine (GEE) was used for all remote sensing data acquisition and calculations (Gorelick et al., 2017). This study used data from the Moderate Resolution Imaging Spectroradiometer (MODIS), which are collected, processed, and stored by the US National Aeronautics and Space Administration (NASA). Specifically, we used the MODIS Terra surface reflectance product (MOD09GA.006), which has a spatial resolution of 500 m^2 for relevant bands, temporal resolution of 1–2 days, and a period of record from 2000 to the present. We selected the Terra product (as opposed to Aqua) since its morning passage would minimize the likelihood of significant cloud formation during image capture; MOD09GA.006 was chosen to remove atmospheric scattering and adsorption that are present in the top of atmosphere product (Vermote and Wolfe, 2015).

Site boundaries were delineated in GEE using field-based knowledge of the spatial configuration of vegetation communities; at the upstream Texas and Louisiana sites visual differences in forest species phenology and physiology between target (CFS species) and non-target areas were used to determine site boundaries. Every MODIS scene during the period from 02/24/2000 to 12/31/2018 was acquired from each site. Clouds were filtered using QA band "state_1km" Bitmask "Bit 10: no cloud" to return pixels that were cloud free for each image. Empty pixels were filtered from each image with band "num_observations_1km", which was set to only return pixels with a value greater than zero. EVI was calculated following Huete et al. (2002):

$$EVI = \frac{\rho_{NIR} - \rho_{red}}{\rho_{NIR} + C_1 \times \rho_{red} - C_2 \times \rho_{blue} + L} \quad (1)$$

where ρ are atmospherically corrected surface reflectance, L is a canopy adjustment factor, and C_1 and C_2 are coefficients of the aerosol resistance term. Coefficient values used were $L = 1$, $C_1 = 6$, $C_2 = 7.5$, and $G = 2.5$ (Huete 1997; Huete et al. 1994). An additional factor of 0.0001 was multiplied against each surface reflectance term to scale results to 1. This process yielded 852 to 1452 images per site. An average EVI was generated for each region of interest per image. (Fig. 3). Finally, any values outside of 2.5 standard deviations (~1.2% of the data) were removed to eliminate anomalous outliers (Miller, 1991). Site elevation data were derived from the Shuttle Radar Topography Mission V3 product (30 m resolution) provided by the NASA Jet Propulsion Laboratory.

2.4. Statistics

All data processing (e.g., temporal subsampling, calculating downstream vs. upstream and growing vs. dormant season EVI ratios) and hypothesis testing was conducted in R (version 3.5.1) using RStudio (version 1.2.1335). Timeseries were generated and subsampled using the eXtensible Times Series package (xts, function; xts, package; Ulrich et al., 2019), slopes were determined using the Sen's slope estimator (sens.slope, trend; Pohlert, 2020), and a Seasonal Decomposition Of Time Series By Loess (stl, stats; Team, 2019) was used for extracting trends. Timeseries slope significance was tested using the Mann-Kendall trend test (MannKendall, Kendall; McLeod, 2011). Data distributions were built using a kernel density estimation (density, stats; Team, 2019) and tested for significance using the Kolmogorov-Smirnov test (ks.test,

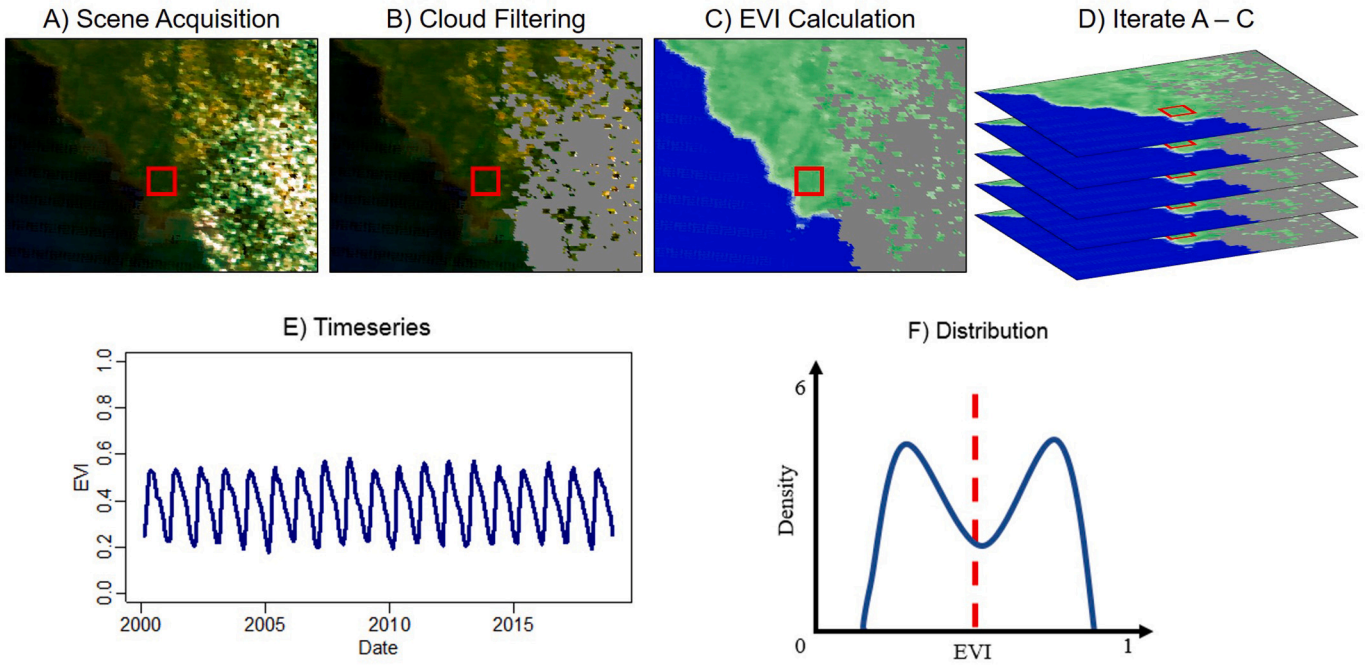

Fig. 3. Workflow for data acquisition: A) Acquire MODIS scene for area of interest, B). Filter image for clouds and empty pixels, C) Calculate EVI on a per-pixel basis and average across the region of interest, D) Iterate steps A-C across the period of interest to create an image collection that can be converted to a timeseries (E) or be analyzed for bulk properties (F).

stats; Team, 2019). Significant differences in median values were assessed using the Mann-Whitney *U* test (wilcox.test, stats; Team, 2019). Downstream, SWI-impacted sites and upstream controls were compared within in each region as well as across the pooled set of upstream and downstream sites. Data were subsampled by different time intervals as needed for each test: weekly for $H_{1A,B}$ and $H_{2A,B}$; monthly for H_{2C} and $H_{3A,B}$; and annual for $H_{3C,D}$ (i.e., annual seasonal ratios derived from monthly data). We used $\alpha = 0.05$ to determine significance for all statistical tests.

3. Results

Median EVI values were significantly lower downstream compared to upstream ($p < 0.001$) for all regions except SE Louisiana (where downstream EVI was significantly higher), partially supporting H_{1A} (Fig. 4). Among regions, median downstream EVI varied more widely (from a low of 0.29 at Suwannee to a maximum of 0.43 in SE Louisiana) than upstream EVI (which ranged from 0.37 to 0.43), indicating greater variation in vegetation conditions across SWI-impacted sites relative to selected controls. There were statistical differences between upstream

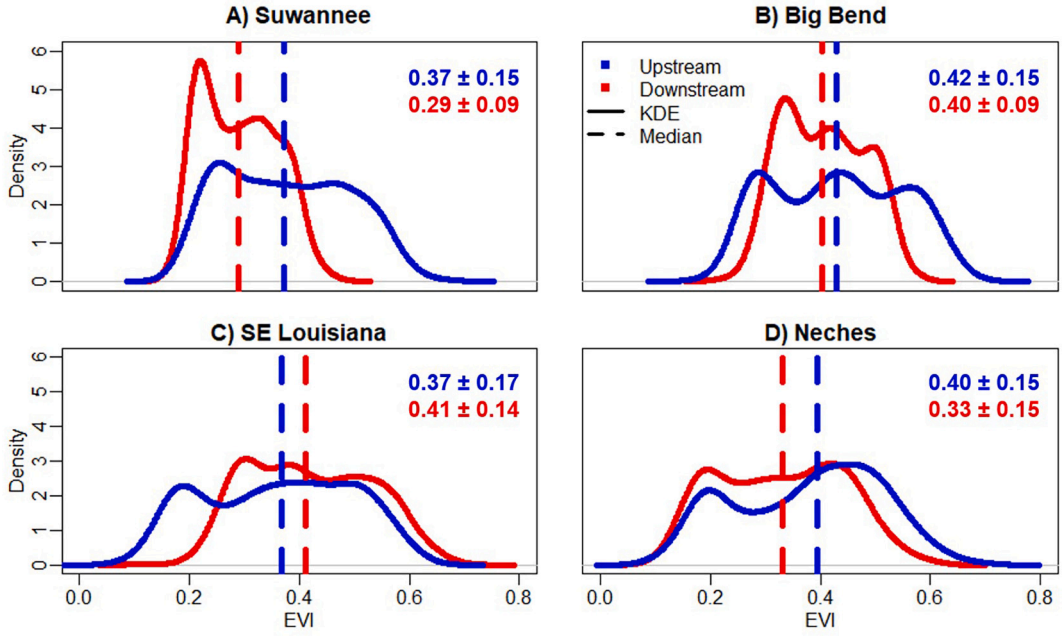

Fig. 4. Distribution of EVI data used for testing Hypotheses H_{1A} and H_{1B}. There was a significant difference between upstream and downstream median (± median absolute deviation) EVI and distribution at all sites (A-D). However, median EVI was greater downstream in SE Louisiana (C), contrary to expectations.

and downstream EVI distributions ($p < 0.001$) in all regions, supporting H_{1B}. Downstream sites tended to have narrower distributions as conceptualized in Fig. 2C, however specific distributions varied considerably by region (Fig. 4). For example, low EVI values were less prevalent downstream than upstream at Big Bend and SE Louisiana, in line with expected increases in dormant-season EVI due to encroachment of salt-tolerant understory vegetation, however the opposite was true at Suwannee and Neches. At Suwannee in particular, the downstream EVI distribution was dominated by a very low mode (discussed further below). High EVI values were more prevalent at upstream sites in all regions as expected (Fig. 2C), with the exception of SE Louisiana.

Weekly EVI time series are shown in Fig. 5, with strong seasonal variation apparent across all regions. Expected differences in growing season EVI (i.e., higher upstream) are visually apparent at Suwannee and Big Bend, while expected differences in dormant season EVI (i.e., higher downstream) are most apparent in SE Louisiana and, to a lesser extent, in the Big Bend. In Neches, growing season EVI at the downstream site fell consistently below the upstream site beginning in 2009. Expected negative EVI trends at downstream sites (H_{2A}) were only significant for Suwannee (Fig. 5A). The only other significant trend was a decrease in upstream EVI in SE Louisiana (Fig. 5C).

Pooled EVI data (Fig. 6) demonstrate that differences between upstream and downstream EVI across regions match our general assumptions regarding CFS structure and dynamics (i.e., downstream sites have lower medians, narrower distributions, and higher dormant season and lower growing season values). The timeseries of pooled data demonstrate that differences in seasonality and growth dynamics are consistent on a long timescale (Fig. 6A). For the average year, both datasets reflected our expectations of differences in deciduous phenology, with the pooled downstream data having a lower amplitude due to differences in seasonal growth patterns, including higher growing season EVI and lower dormant-season EVI downstream (Fig. 6B). Median EVI ($\pm$ median absolute deviation) was significantly lower (0.36 ± 0.11) for pooled downstream sites compared to upstream (0.40 ± 0.14), in addition to having a statistically different distribution (Fig. 6C). Finally, when considering all sites together, EVI distributions of downstream sites had considerably greater-region-to-region variation than upstream sites (Fig. 7).

Only a subset of the nine hypotheses tested here were supported by the remote sensing data, with considerable variation in outcomes across regions (Table 3). Hypotheses were most likely to be supported in the Suwannee River floodplain, which had seven of nine expected outcomes, followed by the Big Bend, Neches, and SE Louisiana sites (with five, four, and three of nine expected outcomes, respectively). Overall, just over half of the full set of hypotheses were supported across regions. The most supported hypotheses ($\geq$ 75% across regions) were H_{1A}, H_{1B}, H_{3A}, and H_{3C}. This subset of best-supported tests identified 81.3% of SWI-stressed sites across regions, with the best performance for the Suwannee River and Big Bend regions (100%), followed by the Neches River (75%), and SE Louisiana (50%; Table 3).

Hypothesis H_{1A}, which tested for expected differences in median EVI between upstream and downstream sites was supported at three of four of regions; the exception was SE Louisiana, where median downstream EVI was significantly greater than upstream (Fig. 4C). Hypothesis H_{1B} was supported at all regions, with differences in EVI distributions across sites described above. Hypothesis H_{2A} was unsupported across all regions, with no significant downstream slopes (Fig. 3), however there was a significantly negative deseasonalized trend (H_{2C}) at the Suwannee downstream site. H_{2B}, which tested for significant declines in the ratio of downstream to upstream EVI, was supported in two regions (Suwannee and Neches). Hypotheses H_{3A} and H_{3c}, which examined differences in median growing season EVI and the ratio of growing to dormant season EVI, respectively, were both supported at three of four regions, while expected differences in median dormant season EVI (H_{3B}) were only significant for two regions. Finally, H_{3D} was unsupported at all regions; while the slope of the growing to dormant season EVI ratio was negative at three of four downstream sites, these trends were all insignificant.

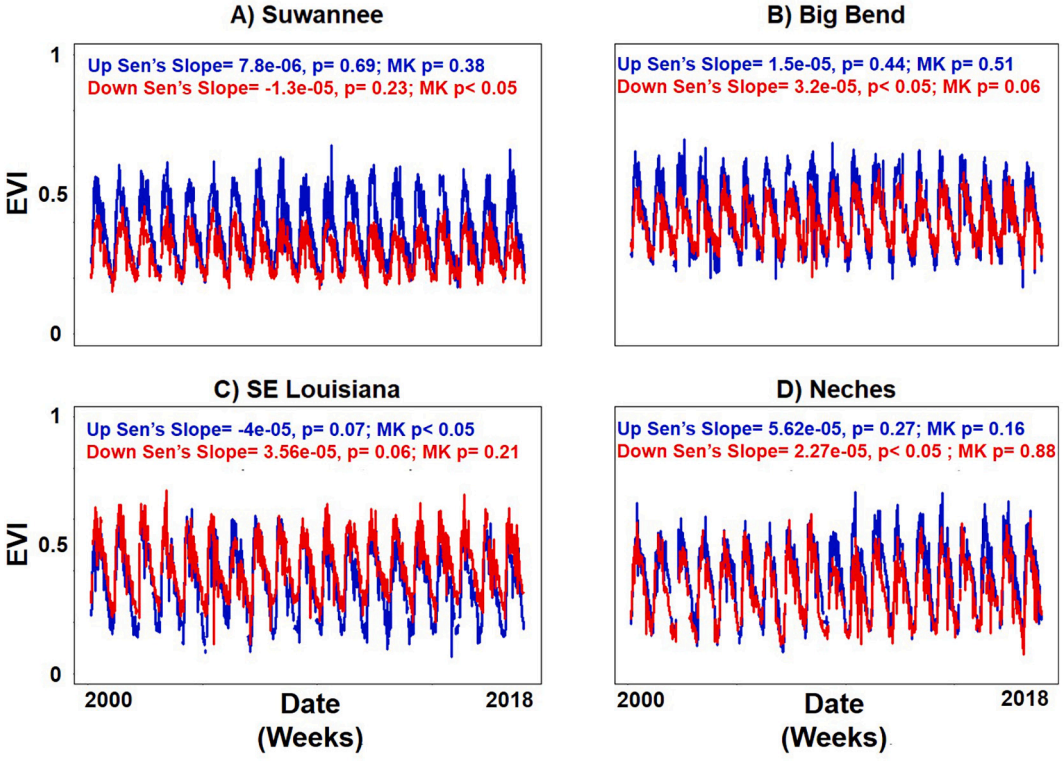

Fig. 5. Weekly EVI timeseries and Mann-Kendall statistics for each site (significant trend lines for Suwannee downstream and SE Louisiana upstream not plotted for visual clarity).

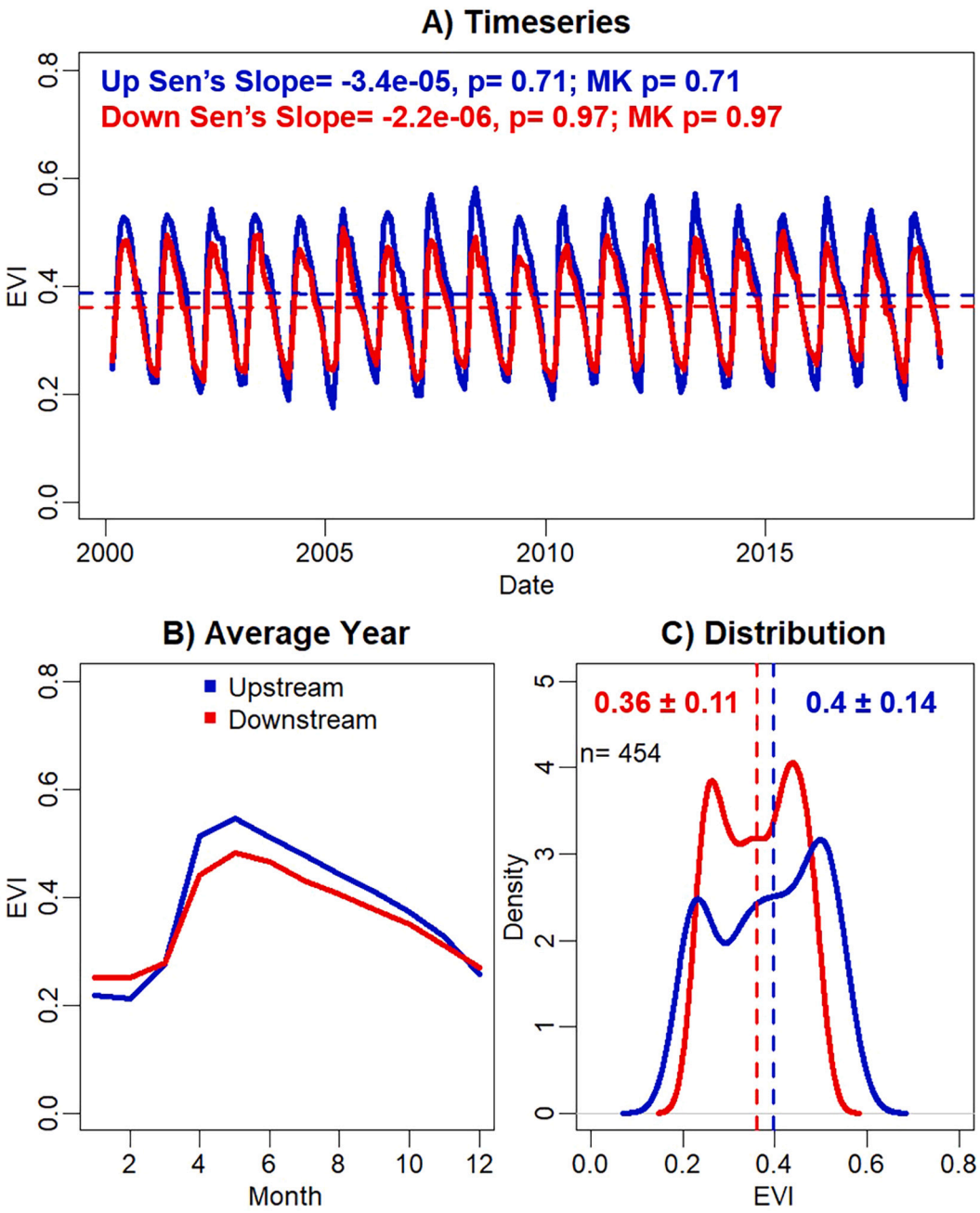

Fig. 6. Pooled upstream and downstream data generally highlight our expected differences in long-term trends, average annual EVI, and EVI distribution.

4. Discussion

Overall, this study demonstrates that remote sensing data can be used to identify CFS impacted by chronic SWI. However, only a subset of the hypotheses we expected to be useful in differentiating impacted sites based on CFS ecology and phenology were supported. The four hypotheses that were most consistently supported by the data (H_{1A}, H_{1B}, H_{3A}, and H_{3C}; supported at 75 to 100% of regions) were all based on EVI summary statistics (i.e., median and distribution). Though derived from timeseries, these statistics do not maintain time-ordered information. In contrast, the least-supported hypotheses (H_{2A}, H_{2B}, H_{2C}, H_{3B}, and H_{3D}; supported at 0 to 50% of regions) relied directly upon the statistics of EVI timeseries (e.g., slope sign and significance of long-term trends). Notably, we found a significantly negative EVI trend for only one of four sites known to be experiencing chronic SWI. While unexpected, there are several potential reasons why temporal hypotheses were less supported, including the slow pace of ecological change driven by chronic SWI (Langston et al., 2017; Williams et al., 2003); seasonal and year-to-year variation in CFS productivity that may mask directional change (Wondie et al., 2007); difference in hydrologic setting and conditions; and unknown specifics of site history not related to SWI (e.g., recovery from historic logging or hurricane disturbance). Below, we apply what we know about the ecological context of SWI-impacted CFS to interpret these results and revisit our hypotheses to synthesize the potential for, and limitations of, EVI-based remote sensing approaches to assessing SWI-impacted systems.

4.1. Best-supported hypotheses

Examining EVI data through the lens of the four most-supported hypotheses (H_{1A}, H_{1B}, H_{3A}, and H_{3C}) reinforces our understanding of several known ecological effects of chronic SWI on CFS. Fundamentally,

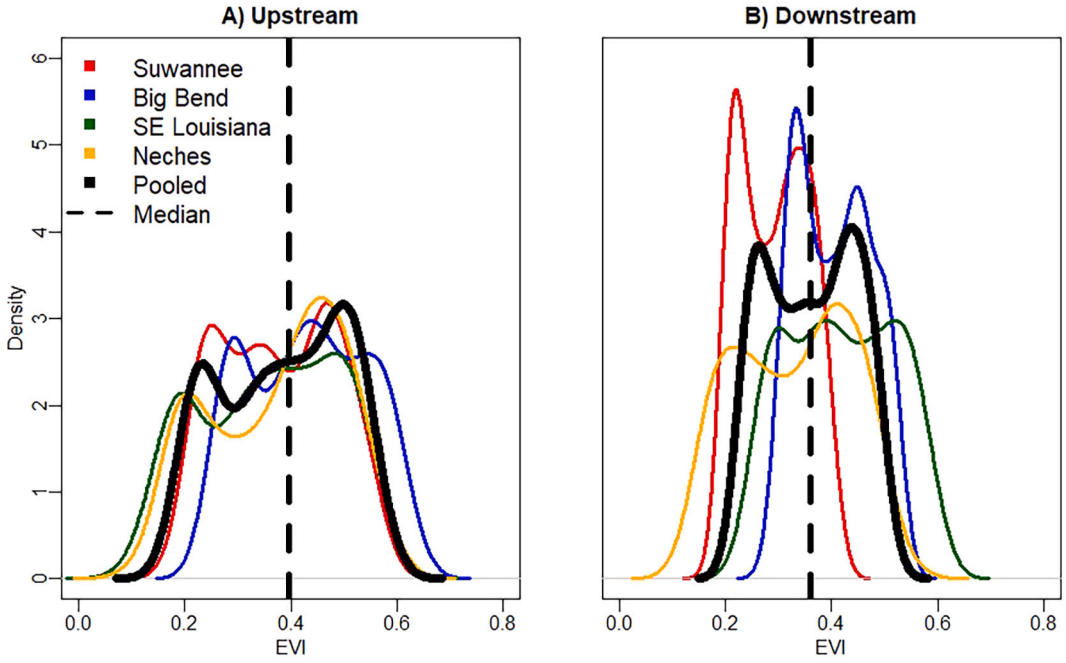

Fig. 7. The distribution of upstream and downstream EVI at all sites, along with their mean (pooled). A) Upstream sites from across the geographic range show similar range and shape compared to the overall mean (black line). B) Downstream sites display a wider variance in range and distribution around the mean downstream distribution.

Table 3
Results of hypothesis testing in each region.

Hypothesis	Suwannee	Big Bend	SE LA	Neches	Support (%)
H_{1A}: $\bar{X}EVI_{DOWN} < \bar{X}EVI_{UP}$	True	True	False	True	75*
H_{1B}: $X \sim EVI_{DOWN} \neq X \sim EVI_{UP}$	True	True	True	True	100*
H_{2A}: Slope $EVI_{DOWN} < 0$	False	False	False	False	0
H_{2C}: Slope $EVI_{Trend,Down} < 0$	True	False	False	False	25
H_{2B}: Slope $EVI_{DOWN:UP} < 0$	True	False	False	True	50
H_{3A}: $\bar{X}EVI_{GS,DOWN} < \bar{X}EVI_{GS,UP}$	True	True	False	True	75*
H_{3B}: $\bar{X}EVI_{DS,DOWN} > \bar{X}EVI_{DS,UP}$	False	True	True	False	50
H_{3C}: $\bar{X}EVI_{GS:DS,DOWN} < \bar{X}EVI_{GS:DS,UP}$	True	True	True	False	75*
H_{3D}: Slope $EVI_{GS:DS,DOWN} < 0$	False	False	False	False	0
All Correct (%)	67	56	33	44	50
Best Supported(%)[a]	100	100	50	75	81

[a] "Best-supported" hypotheses were those supported at ≥75% across regions.

H_{1A} and H_{1B} identify differences in median long-term CFS productivity and phenology, respectively. The reduction of CFS primary productivity by SWI has been demonstrated in the literature (Conner et al., 1997; Cormier et al., 2012; Krauss et al., 2009) and can be quantified relatively simply by comparing long-term median EVI between SWI-impacted and unimpacted sites (H_{1A}; Fig. 3). H_{1A} was supported at all regions except SE Louisiana, and the unique nature of this downstream site is discussed below.

Regarding phenology, H_{1B} provides a long-term summary of the variance, range, and frequency of EVI. Sites unimpacted by SWI should have an EVI distribution with a relatively large range and flat to roughly bi-modal shape driven by the strong seasonality of CFS primary productivity (high in the growing season and very low in the dormant season). EVI distributions in SWI-impacted sites should diverge from unimpacted sites (H_{1B}) due to lower growing season primary productivity and elevated dormant season EVI from the presence of salt-tolerant species into the understory, leading to overall narrower and taller distributions (Figs. 4A-D and 6C). Another potential driver of changes in EVI distributions at SWI-impacted sites is the alteration of leaf emergence and senescence. Specifically, the timing of leaf emergence and senescence has been shown to be affected by direct sodium ion (Na^+) toxicity (Munns, 2002; Yeo and Flowers, 1982). Unlike mangroves or other salt-adapted species, CFS canopy species lack mechanisms to exclude or exude excess salt ions. As such, increasing groundwater salinity could lead to a shift in the timing of leaf emergence and senescence (Brinson et al., 1985; Pezeshki et al., 1988). Hypothesis H_{1B} does not directly identify changes in the timing of leaf emergence and senescence, however future work to quantify CFS phenology using remote sensing could help partition the distributions differences identified here between physiological and phenological effects of SWI.

While H_{1B} was supported at all regions, the specific distribution and direction of "shift" between upstream and downstream varied across regions, challenging the relatively simple conceptualization presented in Fig. 2C. For example, at Suwannee, the downstream distribution was contracted as expected, however it was also shifted to the left rather than toward the middle (Fig. 4A) due to much lower growing-season EVI values (also apparent in Fig. 3A). This phenomenon was likely driven by an abundance of a salt-tolerant herbaceous understory vegetation being detectable through canopy gaps (see site descriptions in SM) and indicates that this site may already be past the successional phase where H_{1B}, as conceived, would serve as an early-warning indicator of ecosystem change. At SE Louisiana, significant differences between upstream and downstream sites also manifested in a way that was unexpected; both dormant and growing season EVI distributions were greater at the downstream site (Figs. 3C and 4C). Here, the presence of *Triadica sebifera*, an aggressive non-native species that is tolerant to salinity (Conner, 1994; USDA, 2018), and *Cephalanthus occidentalis*, a native salinity- and shade-tolerant species (USDA, 2018) may be causing growing season EVI to remain as high, or even higher than, the upstream site. Importantly, EVI values at the upstream site are similar to those at other upstream sites (Fig. 7A), and several metrics of forest quality

measured by CRMS (Wood et al., 2017) indicate that the site is healthy, suggesting that it is the dynamics of the downstream that are an outlier in terms of expected ecosystem responses to SWI. This finding reinforces the need for site-specific knowledge to validate remote sensing approaches applied across wide and diverse spatial domains (Mueller-Warrant et al., 2015; Satyanarayana et al., 2011; Srivastava et al., 2012).

The other two best-supported hypotheses (H_{3A} and H_{3C}) both also used long-term median EVI values but focused on specific seasons. Hypothesis H_{3A} tested for differences in peak growing season (April through June) EVI between upstream and downstream sites and was supported at all regions except SE Louisiana (for the same reasons noted above). Hypothesis H_{3C} combined expectations about growing- and dormant-season EVI to test for differences in their ratio at upstream vs. downstream sites. Conceptually, the ratio in H_{3C} should serve to "amplify" H_{3A} and H_{3B}. For example, if a downstream site had both lower growing season EVI and higher dormant season EVI than an upstream site, then the difference between the sites' G:D ratio should be proportionally greater than differences between either season compared on its own. Hypothesis H_{3C} was supported at all regions except Neches (Table 2). Notably, EVI at the upstream and downstream Neches sites (and thus their G:D ratios) were relatively similar prior to 2009 but diverged from 2010 onward (Fig. 5D), concomitant with the worst regional drought in 500 years (Nielsen-Gammon, 2012). Post-drought, EVI was considerably lower at the downstream site and only began to recover in 2018, however H_{3C}, applied over the period of record, was unable to statistically detect this change. In this case, the mechanism for SWI-induced EVI change (drought) was relatively abrupt, and would likely be better identified using change-point analysis (Al-Quraishi and Kaplan 2020).

4.2. Least-supported hypotheses

Critical evaluation of the five poorly supported hypotheses (H_{2A}, H_{2B}, H_{2C}, H_{3B}, and H_{3D}) highlights the challenges of interpreting CFS phenological and growth dynamics using remote sensing data. Though used to test different aspects of the EVI data, a common feature of H_{2A}, H_{2B}, H_{2C}, and H_{3D} was that they tested the expectation of negative long-term slope as an indicator of ecological change. Hypotheses H_{2A}, H_{2B}, H_{2C} and H_{3D} were likely unsupported across all regions due to the slow pace of change driven by chronic SWI. Field-based studies that seek to track long-term changes in coastal ecosystem primary productivity (above- and belowground biomass production) and community composition and structure (i.e. species richness, abundance, basal area, leaf area index) have relied upon years of site-specific field surveys to quantify relevant changes (Desantis et al., 2007; Langston et al., 2017; Williams et al., 2003). In addition to the site-specific vegetation data, focused field studies are also able to document changes related to natural and anthropogenic disturbances (i.e. hurricanes or road construction), which may aid in the critical interpretation of results. Remote sensing data analysis and interpretation can be inherently limited by the lack of "on-the-ground" data that may provide crucial context (Buckland and Elston, 1994). Further, remote sensing approaches that rely on the detection of long-term change resulting from a chronic stressor may thus be hard to find or interpret in the absence of site-specific knowledge. Finally, H_{3B}, which sought to differentiate sites based upon dormant season EVI, was supported at only half the regions. It is likely that the transition from CFS to saltmarsh (Brinson et al., 1985) has progressed far enough in these locations that our conceptual model based on deterioration (rather than transition) is no longer applicable. This observation is supported by data that show saltmarshes have low EVI values (around 0.2; Jialin et al., 2011), which is close to the observed values from the Suwannee and Neches downstream sites (see Supplementary Material).

The hypotheses developed for this study were based upon our knowledge of CFS and the effects of chronic SWI, with specific expectations for differences in EVI distribution, growing season dynamics, and long-term trends (Fig. 2). While five of the nine hypotheses were not sufficiently supported across all regions, the data do validate our conceptual understanding when pooled (Fig. 6). In particular, Fig. 5A shows a narrowing of the range for the downstream sites and a lower median value, which indicates a decline in the seasonality driven by vegetation shifts and reduction in biomass driven by SWI-induced stress. Fig. 6B shows more specifically the expected differences in seasonality driven by chronic SWI, and Fig. 6C illustrates the consistency of these patterns over long timescales.

5. Methodological considerations and future applications

There are a wide variety of remote sensing products that can be used for earth observation, however Landsat and MODIS are the two primary, publicly available, moderate-resolution datasets. Landsat has a 30 m spatial resolution with a 16 day period of return from 1984 to the present (with red, blue, and near-infrared bands needed for EVI), while MODIS offers greater temporal resolution (1–2 return) with lower spatial resolution (250 m, 500 m, and 1 km) from 2000 to the present. Though Landsat's longer period of record might uncover slower changes associated with chronic SWI, we choose to use MODIS in this analysis because the temporal resolution offered more flexibility to examine CFS effects from the weekly to yearly timescale. In addition to Landsat and MODIS, the European Space Agency's Sentinel 2 mission has a 10-m pixel size (red, green, blue, and near-infrared), and 5-day return period, however its period of record only begins in 2015. Advances in remote sensing and computing power have made it easier to fuse datasets to optimize spatial and temporal resolution (Ghamisi et al., 2019; Luo et al., 2018; Zhang, 2010). NASA has produced several harmonized Landsat 8 and Sentinel 2 products that may give superior inferences to either standalone dataset (Claverie et al., 2018). Recent technological advances in satellite and optical sensors are also reducing the optimization challenge of spatial resolution and periodicity. For example, Planet Labs offers several datasets with 5-m or less spatial resolution and daily coverage, however the data are behind a paywall.

A challenge for wider application of our approach comes from the use of paired sites to underpin local expectations for unimpacted-CFS and those experiencing chronic SWI. Researchers and land managers interested in studying SWI may only have the resources to monitor a site they suspect of being impacted but lack a local, unimpacted site with long-term monitoring to assess results. This challenge could be overcome by using a classification scheme that directly identifies CFS experiencing SWI using a specific spectral signature. However, Fig. 6 highlights potential challenges inherent in this approach. Specifically, while upstream site EVI distributions are variable, each resembles the overall upstream average (Fig. 6A). EVI distributions from downstream sites (Fig. 6B) on the other hand, vary widely, suggesting that a classifier built using training data from a large geographic region may struggle to properly define the boundaries of each class given inherent variance within the data. Additional inputs would be needed to aid in the development of a robust, global classifier; if successfully developed, such a scheme would remove the need for a paired upstream-downstream approach and associated interpretation of statistical comparisons.

Finally, the finding that our best-supported hypotheses relied on summary statistics rather than measures of change over time reinforces that consistent differences exist between upstream and downstream sites; however, these differences—on their own—do not confirm the presence of saltwater intrusion as an active process. In the absence of other information, the differences in EVI observed here could also be attributable to differences in *setting* (i.e., locations closer to the coast experience more chronically stressful, but stationary, conditions relative to upstream sites) rather than as an *outcome* of active SWI. However, current rates of SLR and many field-based studies support the idea that chronic SWI is a process that is actively driving the degradation of CFS along the northern Gulf of Mexico (Desantis et al., 2007; Langston et al., 2017; Middleton et al., 2015; Raabe and Stumpf, 2016; Williams et al.,

1999). In either case, the downstream sites selected for this study all had consistent records of groundwater salinity elevated above ideal conditions for CFS and thus represent a likely future state for fresher systems upstream; here we showed that remote sensing data could be used to identify these systems across a range of salinity, management, vegetation, and site history settings. The reliability of the best-supported hypotheses supports their wider application across the northern Gulf of Mexico. For example, recent analysis completed using remote sensing data quantified 172,147 km^2 of CFS in 1996, with 19,480 km^2 (11%) lost between 1996 and 2016 (White et al., submitted for publication). At this rate of loss (974 km^2/yr) CFS may not exist far into next century, further demonstrating the need to actively track the health of these systems for immediate intervention.

Credit author statement

Elliott White Jr.: Conceptualization, Methodology, Software, Validation, Formal analysis, Investigation, Data curation, Writing – Original Draft, Writing – Review & Editing, Visualization.

David Kaplan.: Conceptualization, Methodology, Writing – Review & Editing, Supervision.

Declaration of Competing Interest

The authors have no competing interest.

Acknowledgemnts

The authors thank Dr. Beth Middleton and Evelyn Anemaet of the USGS National Wetlands and Aquatic Research Center for the research opportunity and field insights provided. Hydrologic and water quality data for the Neches River were provided by the Lower Neches Valley Authority. Dr. Alice Alonso of UCLouvain and Dr. Katie Glodzik of the University of Florida provided advice making the work possible in Google Earth Engine. Finally, the Watershed Ecology Lab at the University of Florida (UF) provided methodological critiques and served as the first (and second and third…) review panel. Financial support was provided through the UF Graduate Student Fellowship, Glick Graduate Scholarship, and Melnick Scholarship Award made this work possible.

Appendix A. Supplementary data

Supplementary data to this article can be found online at https://doi.org/10.1016/j.rse.2021.112385.

References

Allen, J.A., Chambers, J.L., Pezeshki, S.R., 1997. Effects of salinity on baldcypress seedlings: physiological responses and their relation to salinity tolerance. Wetlands 17, 310–320. https://doi.org/10.1007/Bf03161419.

Alonso, A., Munoz-Carpena, R., Kennedy, R.E., Murcia, C., 2016. Wetland landscape spatio-temporal degradation dynamics using the new Google earth engine cloud-based platform: opportunities for non-specialists in remote sensing. Trans. ASABE 59, 1333–1344. https://doi.org/10.13031/trans.59.11608.

Angelini, C., Silliman, B.R., 2012. Patch size-dependent community recovery after massive disturbance. Ecology 93, 101–110. https://doi.org/10.1890/11-0557.1.

Blair, S., Adams, C., Ankerson, T., McGuire, M., Kaplan, D., 2015. Ecosystem Services Valuation for Estuarine and Coastal Restoration in Florida. Florida Sea Grant/University Florida Inst. Food Agric. Sci. Electron. Data Inf. Source.

Brinson, M.M., Bradshaw, H.D., Holmes, R.N., Elkins, J.B., 1980. Litterfall, stemflow, and throughfall nutrient fluxes in an alluvial swamp forest. Ecology 61, 827–835. https://doi.org/10.2307/1936753.

Brinson, M.M., Bradshaw, H.D., Jones, M.N., 1985. Transitions in forested wetlands along gradients of salinity and hydroperiod. J. Elisha Mitchell Sci. Soc. 101, 76.

Brinson, M.M., Christian, R.R., Blum, L.K., 1995. Multiple states in the sea-level induced transition from terrestrial forest to estuary. Estuaries 18, 648–659. https://doi.org/10.2307/1352383.

Buckland, S.T., Elston, D.A., 1994. Use of groundtruth data to correct land-cover area estimates from remotely-sensed data. Int. J. Remote Sens. 15, 1273–1282. https://doi.org/10.1080/01431169408954160.

Cahoon, D.R., Lynch, J.C., Roman, C.T., Schmit, J.P., Skidds, D.E., 2019. Evaluating the relationship among wetland vertical development, elevation capital, sea-level rise, and tidal marsh sustainability. Estuar. Coasts 42, 1–15. https://doi.org/10.1007/s12237-018-0448-x.

Charles, S.P., Kominoski, J.S., Troxler, T.G., Gaiser, E.E., Servais, S., Wilson, B.J., Davis, S.E., Sklar, F.H., Coronado-Molina, C., Madden, C.J., Kelly, S., Rudnick, D.T., 2019. Experimental saltwater intrusion drives rapid soil elevation and carbon loss in freshwater and Brackish everglades marshes. Estuar. Coasts 42, 1868–1881. https://doi.org/10.1007/s12237-019-00620-3.

Chen, W., Chen, K., Kuang, C., Zhu, D.Z., He, L., Mao, X., Liang, H., Song, H., 2016. Influence of sea level rise on saline water intrusion in the Yangtze River Estuary, China. Appl. Ocean Res. 54, 12–25. https://doi.org/10.1016/j.apor.2015.11.002.

Church, J.A., White, N.J., 2011. Sea-level rise from the late 19th to the early 21st century. Surv. Geophys. 32, 585–602. https://doi.org/10.1007/s10712-011-9119-1.

Claverie, M., Ju, J., Masek, J.G., Dungan, J.L., Vermote, E.F., Roger, J.-C., Skakun, S.V., Justice, C., 2018. The harmonized Landsat and Sentinel-2 surface reflectance data set. Remote Sens. Environ. 219, 145–161. https://doi.org/10.1016/j.rse.2018.09.002.

Conner, W.H., 1994. The effect of salinity and waterlogging on growth and survival of Baldcypress and Chinese tallow seedlings. J. Coast. Res. 10, 1045–1049.

Conner, W.H., 1995. Woody plant regeneration in three South Carolina Taxodium/Nyssa stands following Hurricane Hugo. Ecol. Eng. 4, 277–287. https://doi.org/10.1016/0925-8574(94)00054-9.

Conner, W.H., McLeod, K.W., McCarron, J.K., 1997. Flooding and salinity effects on growth and survival of four common forested wetland species. Wetl. Ecol. Manag. 5, 99–109. https://doi.org/10.1023/a:1008251127131.

Cormier, N., Krauss, K.W., Conner, W.H., 2012. Periodicity in stem growth and litterfall in tidal freshwater forested wetlands: influence of salinity and drought on nitrogen recycling. Estuar. Coasts 36, 533–546. https://doi.org/10.1007/s12237-012-9505-z.

Costanza, R., de Groot, R., Sutton, P., van der Ploeg, S., Anderson, S.J., Kubiszewski, I., Farber, S., Turner, R.K., 2014. Changes in the global value of ecosystem services. Glob. Environ. Chang. Policy Dimens. 26, 152–158. https://doi.org/10.1016/j.gloenvcha.2014.04.002.

Cowardin, L.M., Carter, V., Golet, F.C., LaRoe, E.T., 1979. Classification of Wetlands and Deepwater Habitats of the United States.

Craft, C., 2012. Tidal freshwater forest accretion does not keep pace with sea level rise. Glob. Chang. Biol. 18, 3615–3623.

Craft, C., Clough, J., Ehman, J., Joye, S., Park, R., Pennings, S., Guo, H.Y., Machmuller, M., 2009. Forecasting the effects of accelerated sea-level rise on tidal marsh ecosystem services. Front. Ecol. Environ. 7, 73–78. https://doi.org/10.1890/070219.

Desantis, L.R.G., Bhotika, S., Williams, K., Putz, F.E., 2007. Sea-level rise and drought interactions accelerate forest decline on the Gulf Coast of Florida, USA. Glob. Chang. Biol. 13, 2349–2360. https://doi.org/10.1111/j.1365-2486.2007.01440.x.

Doyle, T.W., O'Neil, C.P., Melder, M.P.V., From, A.S., Palta, M.M., 2007. Tidal Freshwater Swamps of the Southeastern United States: Effects of Land Use, Hurricanes, Sea-Level Rise, and Climate Change, in: Ecology of Tidal Freshwater Forested Wetlands of the Southeastern United States. Springer Netherlands, Dordrecht, pp. 1–28. https://doi.org/10.1007/978-1-4020-5095-4_1.

Duchemin, B., Goubier, J., Courrier, G., 1999. Monitoring phenological key stages and cycle duration of temperate deciduous forest ecosystems with NOAA/AVHRR data. Remote Sens. Environ. 67, 68–82. https://doi.org/10.1016/S0034-4257(98)00067-4.

Engle, V.D., 2011. Estimating the provision of ecosystem services by Gulf of Mexico coastal wetlands. Wetlands 31, 179–193. https://doi.org/10.1007/s13157-010-0132-9.

Franklin, J.F., 1989. Importance and justification of long-term studies in ecology. In: Long-Term Studies in Ecology. Springer, pp. 3–19.

Ghamisi, P., Gloaguen, R., Atkinson, P.M., Benediktsson, J.A., Rasti, B., Yokoya, N., Wang, Q., Hofle, B., Bruzzone, L., Bovolo, F., Chi, M., Anders, K., 2019. Multisource and multitemporal data fusion in remote sensing: a comprehensive review of the state of the art. IEEE Geosci. Remote Sens. Mag. 7, 6–39. https://doi.org/10.1109/mgrs.2018.2890023.

Goldberg, L., Lagomasino, D., Thomas, N., Fatoyinbo, T., 2020. Global declines in human-driven mangrove loss. Glob. Chang. Biol. https://doi.org/10.1111/gcb.15275.

Gorelick, N., Hancher, M., Dixon, M., Ilyushchenko, S., Thau, D., Moore, R., 2017. Google earth engine: planetary-scale geospatial analysis for everyone. Remote Sens. Environ. 202, 18–27. https://doi.org/10.1016/j.rse.2017.06.031.

Hall, R.B.W., Harcombe, P.A., 1998. Flooding alters apparent position of floodplain saplings on a light gradient. Ecology 79, 847–855. https://doi.org/10.1890/0012-9658(1998)079[0847:faapof]2.0.co;2.

Hong, M.G., Nam, B.E., Kim, J.G., 2019. Changes in vegetation and flora of abandoned paddy terraces in responses to drawdown. J. Ecol. Environ. 43, 22. https://doi.org/10.1186/s41610-019-0120-9.

Horton, B.P., Rahmstorf, S., Engelhart, S.E., Kemp, A.C., 2014. Expert assessment of sea-level rise by AD 2100 and AD 2300. Quat. Sci. Rev. 84, 1–6. https://doi.org/10.1016/j.quascirev.2013.11.002.

Huenneke, L.F., Sharitz, R.R., 1986. Microsite abundance and distribution of Woody seedlings in a South Carolina cypress-tupelo swamp. Am. Midl. Nat. 115, 328. https://doi.org/10.2307/2425869.

Ji, C.Y., Liu, Q.H., Sun, D.F., Wang, S., Lin, P., Li, X.W., 2001. Monitoring urban expansion with remote sensing in China. Int. J. Remote Sens. 22, 1441–1455. https://doi.org/10.1080/01431160117207.

Jialin, L., Hanbing, Z., Xiaoping, Y., 2011. Study on the seasonal dynamics of zonal vegetation of NDVI/EVI of costal zonal vegetation based on MODIS data: a case study of Spartina alterniflora salt marsh on Jiangsu Coast, China. Afr. J. Agric. Res. 6, 4019–4024.

Kaplan, D., Munoz-Carpena, R., Wan, Y., Hedgepeth, M., Zheng, F., Roberts, R., Rossmanith, R., 2010. Linking river, floodplain, and vadose zone hydrology to improve restoration of a coastal river affected by saltwater intrusion. J. Environ. Qual. 39, 1570–1584. https://doi.org/10.2134/jeq2009.037510.2134/jeq2009.0375.

Kirwan, M.L., Gedan, K.B., 2019. Sea-level driven land conversion and the formation of ghost forests. Nat. Clim. Chang. 9, 450–457. https://doi.org/10.1038/s41558-019-0488-7.

Kirwan, M.L., Walters, D.C., Reay, W.G., Carr, J.A., 2016. Sea level driven marsh expansion in a coupled model of marsh erosion and migration. Geophys. Res. Lett. 43, 4366–4373. https://doi.org/10.1002/2016gl068507.

Klein, E., Berg, E.E., Dial, R., 2005. Wetland drying and succession across the Kenai Peninsula Lowlands, south-central Alaska. Can. J. For. Res. Can. Rech. For. 35, 1931–1941. https://doi.org/10.1139/x05-129.

Knighton, A.D., Mills, K., Woodroffe, C.D., 1991. Tidal-Creek extension and saltwater intrusion in Northern Australia. Geology 19, 831–834. https://doi.org/10.1130/0091-7613(1991)019<0831:Tceasi>2.3.Co;2.

Krauss, K.W., Duberstein, J.A., Doyle, T.W., Conner, W.H., Day, R.H., Inabinette, L.W., Whitbeck, J.L., 2009. Site condition, structure, and growth of Baldcypress along tidal/non-tidal salinity gradients. Wetlands 29, 505–519. https://doi.org/10.1672/08-77.1.

Krauss, K.W., Duberstein, J.A., Conner, W.H., 2015. Assessing stand water use in four coastal wetland forests using sapflow techniques: annual estimates, errors and associated uncertainties. Hydrol. Process. 29, 112–127. https://doi.org/10.1002/hyp.10130.

Krauss, K.W., Holm Jr., G.O., Perez, B.C., McWhorter, D.E., Cormier, N., Moss, R.F., Johnson, D.J., Neubauer, S.C., Raynie, R.C., 2016. Component greenhouse gas fluxes and radiative balance from two deltaic marshes in Louisiana: pairing chamber techniques and eddy covariance. J. Geophys. Res. Biogeosci. 121, 1503–1521. https://doi.org/10.1002/2015JG003224.

Krauss, K.W., From, A.S., Rogers, C.S., Whelan, K.R.T., Grimes, K.W., Dobbs, R.C., Kelley, T., 2020. Structural Impacts, Carbon Losses, and Regeneration in Mangrove Wetlands after Two Hurricanes on St. John. U.S. Virgin Islands, Wetlands. https://doi.org/10.1007/s13157-020-01313-5.

Langston, A.K., Kaplan, D.A., Putz, F.E., 2017. A casualty of climate change? Loss of freshwater forest islands on Florida's Gulf Coast. Glob. Chang. Biol. 23, 5383–5397. https://doi.org/10.1111/gcb.1380510.1111/gcb.13805 (Epub 2017 Jul 26).

Li, G., Weng, Q., 2007. Measuring the quality of life in city of Indianapolis by integration of remote sensing and census data. Int. J. Remote Sens. 28, 249–267. https://doi.org/10.1080/01431160600735624.

Liu, X.J., Conner, W.H., Song, B., Jayakaran, A.D., 2017. Forest composition and growth in a freshwater forested wetland community across a salinity gradient in South Carolina USA. For. Ecol. Manag. 389, 211–219. https://doi.org/10.1016/j.foreco.2016.12.022.

Lovett, G.M., Burns, D.A., Driscoll, C.T., Jenkins, J.C., Mitchell, M.J., Rustad, L., Shanley, J.B., Likens, G.E., Haeuber, R., 2007. Who needs environmental monitoring? Front. Ecol. Environ. 5, 253–260. https://doi.org/10.1890/1540-9295(2007)5[253:wnem]2.0.co;2.

Luo, Y., Guan, K., Peng, J., 2018. STAIR: a generic and fully-automated method to fuse multiple sources of optical satellite data to generate a high-resolution, daily and cloud−/gap-free surface reflectance product. Remote Sens. Environ. 214, 87–99. https://doi.org/10.1016/j.rse.2018.04.042.

Magnuson, J.J., 1990. Long-term ecological research and the invisible present - uncovering the processes hidden because they occur slowly or because effects lag years behind causes. Bioscience 40, 495–501. https://doi.org/10.2307/1311317.

Magolan, J.L., Halls, J.N., 2020. A multi-decadal investigation of Tidal Creek wetland changes, water level rise, and ghost forests. Remote Sens. 12, 1141.

McKee, K.L., Mendelssohn, I.A., 1989. Response of a freshwater marsh plant community to increased salinty and increased water level. Aquat. Bot. 34, 301–316.

McLeod, A.I., 2011. Kendall: Kendall Rank Correlation and Mann-Kendall Trend Test.

Middleton, B.A., Souter, N.J., 2017. Functional integrity of freshwater forested wetlands, hydrologic alteration, and climate change. Ecosyst. Heal. Sustain. 2, e01200 https://doi.org/10.1002/ehs2.1200.

Middleton, B.A., Johnson, D., Roberts, B.J., 2015. Hydrologic remediation for the Deepwater horizon incident drove ancillary primary production increase in coastal swamps. Ecohydrology 8, 838–850. https://doi.org/10.1002/eco.1625.

Miller, J., 1991. Short report: reaction time analysis with outlier exclusion: Bias varies with sample size. Q. J. Exp. Psychol. Sect. A 43, 907–912. https://doi.org/10.1080/14640749108400962.

Mitsch, W., Gosselink, J., 2015. Wetlands, 5th edition. John Wiley & Sons, Inc.

Moran, M.S., Inoue, Y., Barnes, E.M., 1997. Opportunities and limitations for image-based remote sensing in precision crop management. Remote Sens. Environ. 61, 319–346. https://doi.org/10.1016/S0034-4257(97)00045-X.

Morris, J.T., Sundareshwar, P.V., Nietch, C.T., Kjerfve, B., Cahoon, D.R., 2002. Responses of coastal wetlands to rising sea level. Ecology 83, 2869–2877. https://doi.org/10.1890/0012-9658(2002)083[2869:rocwtr]2.0.co;2.

Mueller-Warrant, G.W., Whittaker, G.W., Banowetz, G.M., Griffith, S.M., Barnhart, B.L., 2015. Methods for improving accuracy and extending results beyond periods covered by traditional ground-truth in remote sensing classification of a complex landscape. Int. J. Appl. Earth Obs. Geoinf. 38, 115–128. https://doi.org/10.1016/j.jag.2015.01.001.

Munns, R., 2002. Comparative physiology of salt and water stress. Plant Cell Environ. 25, 239–250.

Nakaji, T., Oguma, H., Hiura, T., 2011. Ground-based monitoring of the leaf phenology of deciduous broad-leaved trees using high resolution NDVI camera images. J. Agric. Meteorol. 67, 65–74. https://doi.org/10.2480/agrmet.67.2.3.

Neubauer, S.C., 2011. Ecosystem responses of a tidal freshwater marsh experiencing saltwater intrusion and altered hydrology. Estuar. Coasts 36, 491–507. https://doi.org/10.1007/s12237-011-9455-x.

Nielsen-Gammon, J.W., 2012. The 2011 Texas Drought, 3, p. 37.

Odland, A., del Moral, R., 2002. Thirteen years of wetland vegetation succession following a permanent drawdown, Myrkdalen Lake, Norway. Plant Ecol. 162, 185–198. https://doi.org/10.1023/A:1020388910724.

Pezeshki, S.R., Delaune, R.D., Patrick, W.H., 1988. Effect of salinity on leaf ionic content and photosynthesis of Taxodium-Distichum L. Am. Midl. Nat. 119, 185–192. https://doi.org/10.2307/2426067.

Pierfelice, K.N., Lockaby, B.G., Krauss, K.W., Conner, W.H., Noe, G.B., Ricker, M.C., Graeme Lockaby, B., Krauss, K.W., Conner, W.H., Noe, G.B., Ricker, M.C., 2015. Salinity influences on aboveground and belowground net primary productivity in tidal wetlands. J. Hydrol. Eng. 22, D5015002 https://doi.org/10.1061/(Asce)He.1943-5584.0001223.

Pohlert, T., 2020. Trend: Non-Parametric Trend Tests and Change-Point Detection https://doi.org/https://cran.r-project.org/web/packages/trend/trend.pdf.

Raabe, E.A., Stumpf, R.P., 2016. Expansion of tidal marsh in response to sea-level rise: Gulf Coast of Florida, USA. Estuar. Coasts 39, 145–157. https://doi.org/10.1007/s12237-015-9974-y.

Rasmussen, P., Sonnenborg, T.O., Goncear, G., Hinsby, K., 2013. Assessing impacts of climate change, sea level rise, and drainage canals on saltwater intrusion to coastal aquifer. Hydrol. Earth Syst. Sci. 17, 421–443. https://doi.org/10.5194/hess-17-421-2013.

Reaver, N.G.F., Kaplan, D.A., Mattson, R.A., Carter, E., Sucsy, P.V., Frazer, T.K., 2019. Hydrodynamic controls on primary producer communities in spring-fed rivers. Geophys. Res. Lett. 46, 4715–4725. https://doi.org/10.1029/2019gl082571.

Rice, K.C., Hong, B., Shen, J., 2012. Assessment of salinity intrusion in the James and Chickahominy Rivers as a result of simulated sea-level rise in Chesapeake Bay, East Coast, USA. J. Environ. Manag. 111, 61–69. https://doi.org/10.1016/j.jenvman.2012.06.03610.1016/j.jenvman.2012.06.036 (Epub 2012 Jul 20).

Robertson, J.M., Augspurger, C.K., 1999. Geomorphic processes and spatial patterns of primary forest succession on the Bogue Chitto River, USA. J. Ecol. 87, 1052–1063. https://doi.org/10.1046/j.1365-2745.1999.00416.x.

Ross, M.S., Obrien, J.J., Sternberg, L.D.L., 1994. Sea-level rise and the reduction in pine forests in the Florida keys. Ecol. Appl. 4, 144–156. https://doi.org/10.2307/1942124.

Ryberg, K.R., Vecchia, A.V., 2012. waterData: Retrieval, Analysis, and Anomaly Calculation of Daily Hydrologic Time Series Data.

Satyanarayana, B., Mohamad, K.A., Idris, I.F., Husain, M.-L., Dahdouh-Guebas, F., 2011. Assessment of mangrove vegetation based on remote sensing and ground-truth measurements at Tumpat, Kelantan Delta, East Coast of Peninsular Malaysia. Int. J. Remote Sens. 32, 1635–1650. https://doi.org/10.1080/01431160903586781.

Schemel, L.E., 2001. Simplified conversions between specific conductance and salinity units for use with data from monitoring stations. Interag. Ecol. Progr. Newsl. 14, 17–18.

Schieder, N.W., Walters, D.C., Kirwan, M.L., 2018. Massive upland to wetland conversion compensated for historical marsh loss in Chesapeake Bay, USA. Estuar. Coasts 41, 940–951. https://doi.org/10.1007/s12237-017-0336-9.

Srivastava, P.K., Han, D., Rico-Ramirez, M.A., Bray, M., Islam, T., 2012. Selection of classification techniques for land use/land cover change investigation. Adv. Sp. Res. 50, 1250–1265. https://doi.org/10.1016/j.asr.2012.06.032.

Steyer, G.D., Perez, B.C., Piazza, S., Suir, G., 2007. Potential consequences of saltwater intrusion associated with hurricanes Katrina and Rita. In: Farris, G.S., Smith, G.J., Crane, M.P., Demas, C.R., Robbins, L.L., Lavoie, D.L. (Eds.), Science and the Storms: The USGS Response to the Hurricanes of 2005. U.S. Geological Survey, Reston, VA, pp. 137–146.

Strayer, D., Glitzenstein, J.S., Jones, C.G., Kolasa, J., Likens, G.E., McDonnell, M.J., Parker, G.G., Pickett, S.T.A., 1986. Long-term ecological studies: an illustrated account of their design, operation, and importance to ecology. Occas. Publ. Inst. Ecosyst. Stud. 2.

Taillie, P., Roman-Cuesta, R., Lagomasino, D., Cifuentes-Jara, M., Fatoyinbo, T.L., Ott, L. E., Poulter, B., 2020. Widespread mangrove damage resulting from the 2017 Atlantic mega hurricane season. In: Environ. Res. Lett.Team, R.C., 2019. R: A Language and Environment for Statistical Computing.

Ulrich, J.M., Ryan, J.A., Bennett, R., Joy, C., 2019. xts: eXtensible Time Series.

Ury, E.A., Anderson, S.M., Peet, R.K., Bernhardt, E.S., Wright, J.P., 2020. Succession, regression and loss: does evidence of saltwater exposure explain recent changes in the tree communities of North Carolina's coastal plain? Ann. Bot. 125, 255–264. https://doi.org/10.1093/aob/mcz039. USDA, N., 2018. The PLANTS database.

USDA, 2018. The PLANTS database. https://doi.org/10.1093/aob/mcz039.

Vermote, E., Wolfe, R., 2015. MOD09GA MODIS/Terra Surface Reflectance Daily L2G Global 1kmand 500m SIN Grid V006 [Data Set]. https://doi.org/10.5067/MODIS/MOD09GA.006.

Wang, Q., Adiku, S., Tenhunen, J., Granier, A., 2005. On the relationship of NDVI with leaf area index in a deciduous forest site. Remote Sens. Environ. 94, 244–255. https://doi.org/10.1016/j.rse.2004.10.006.

White, E., Kaplan, D., 2017. Restore or retreat? Saltwater intrusion and water management in coastal wetlands. Ecosyst. Heal. Sustain. 3, e01258 https://doi.org/10.1002/ehs2.1258.

Williams, K., Ewel, K.C., Stumpf, R.P., Putz, F.E., Workman, T.W., 1999. Sea-level rise and coastal forest retreat on the west coast of Florida, USA. Ecology 80, 2045–2063. https://doi.org/10.1890/0012-9658(1999)080[2045:slracf]2.0.co;2.

Williams, K., MacDonald, M., Sternberg, L.D.L., 2003. Interactions of storm, drought, and sea-level rise on coastal forest: a case study. J. Coast. Res. 19, 1116–1121.

Wondie, A., Mengistu, S., Vijverberg, J., Dejen, E., 2007. Seasonal variation in primary production of a large high altitude tropical Lake (lake Tana, Ethiopia): effects of nutrient availability and water transparency. Aquat. Ecol. 41, 195–207. https://doi.org/10.1007/s10452-007-9080-8.

Wood, W.B., Shaffer, G.P., Visser, J.M., Krauss, K.W., Piazza, S.C., Sharp, L.A., Cretini, K. F., Survey, U.S.G., 2017. Forested floristic quality index: an assessment tool for forested wetland habitats using the quality and quantity of woody vegetation at Coastwide Reference Monitoring System (CRMS) vegetation monitoring stations. In: Open-File Report. Reston, VA. https://doi.org/10.3133/ofr20171002.

Xie, Y., Wilson, A.M., 2020. Change point estimation of deciduous forest land surface phenology. Remote Sens. Environ. 240, 111698. https://doi.org/10.1016/j.rse.2020.111698.

Yeo, A.R., Flowers, T.J., 1982. Accumulation and localization of sodium-ions within the shoots of rice (Oryza-Sativa) varieties differing in salinity resistance. Physiol. Plant. 56, 343–348. https://doi.org/10.1111/j.1399-3054.1982.tb00350.x.

Yin, Y., 1998. Flooding and forest succession in a modified stretch along the Upper Mississippi River. Regul. Rivers-Research Manag. 14, 217–225. https://doi.org/10.1002/(Sici)1099-1646(199803/04)14:2<217::Aid-Rrr499>3.0.Co;2-S.

Zeiringer, B., Seliger, C., Greimel, F., Schmutz, S., 2018. River hydrology, flow alteration, and environmental flow. In: Schmutz, S., Sendzimir, J. (Eds.), Riverine Ecosystem Management: Science for Governing Towards a Sustainable Future. Springer International Publishing, Cham, pp. 67–89. https://doi.org/10.1007/978-3-319-73250-3_4.

Zhang, J., 2010. Multi-source remote sensing data fusion: status and trends. Int. J. Image Data Fusion 1, 5–24. https://doi.org/10.1080/19479830903561035.